DIRECT NUMERICAL SIMULATIONS OF A PASSIVE SCALAR IN A TURBULENT CHANNEL WITH LOCAL FORCING AT WALLS

Guillermo Araya
Department of Mechanical, Aeronautical and Nuclear Engineering,
Rensselaer Polytechnic Institute, Troy, NY, 12180, US
arayaj@rpi.edu

Stefano Leonardi
Department of Mechanical Engineering,
University of Puerto Rico at Mayaguez, Mayaguez, 00680, Puerto Rico, US

Luciano Castillo
Department of Mechanical, Aeronautical and Nuclear Engineering,
Rensselaer Polytechnic Institute, Troy, NY, 12180, US

ABSTRACT

The influence of local forcing on a turbulent channel flow is numerically investigated. The high level of information provided by Direct Numerical Simulations (DNS) allows a better understanding of the physical mechanism responsible for local drag reduction and heat transfer enhancement. The molecular Prandtl number is 0.71 and the Reynolds number based on the wall friction velocity and the channel half width is 394 for the unforced case. A phase-averaging procedure is employed to discriminate between coherent and incoherent structures. It is shown that coherent thermal fluctuations reach peak values near the forcing slot, sharply decay and almost disappear in a short distance downstream. The incoherent thermal fluctuations also show peak values next to the source; however, they decay downstream to look similar as incoherent structures of the unperturbed channel. Budgets for the passive scalar variance and turbulent heat fluxes at a dimensionless forcing frequency of 0.64 are compared with the unforced case budgets. In general, it is observed an increase of all terms when the flow is locally perturbed, especially, in a zone very close to the wall, namely $0 < y^+ < 70$. Local increases on molecular heat fluxes up to 50% are accomplished at a dimensionless frequency of 0.64. Furthermore, wall-normal turbulent heat fluxes experience a significant augmentation (~21%) at this forcing frequency.

INTRODUCTION

Transport of passive scalars in turbulent flows is crucial in many engineering applications such as electronic cooling, combustion, turbine-blade cooling and atmospheric flows. Particular attention has recently been paid to heat transfer enhancement techniques due to the steady increase of heat load in engineering devices. Furthermore, an exhaustive literature review of these techniques was performed by Bergles *et al*. (1995). Passive techniques, such as roughness, extended surfaces or additives, are simple and do not require external power; however, they show limitations to operate efficiently in a wide range of conditions and can not remove a high amount of heat. On the other hand, active techniques may overcome deficiencies of passive techniques when the desired results justify the investment (Gad-el-Hak, 2000). Local forcing is an active technique, which consists on perturbing the flow by a periodic blowing/suction velocity applied in a confined zone over the wall. Several investigations have recently been focused on achieving drag reduction by controlling the coherent structures that arise when a local periodic disturbance is imposed on the flow; Park *et al*. (2003), Park and Sung (2005) and Kim and Sung (2003). In a previous investigation, Araya *et al*. (2007) focused on the effects of local forcing on the velocity field of a turbulent channel by performing Direct Numerical Simulations (DNS) at a Reynolds number, Re_τ, of 180. The maximum local skin friction reduction of 30% was accomplished at the maximum forcing amplitude considered, i.e., A_o = 0.35, and, at a frequency, $\bar{f}$, of 0.04.

Rhee and Sung (2000) numerically predicted the enhancement of heat transfer in locally forced turbulent separated and reattaching flow over a backward-facing step. They extended a version of the k-ε-f_μ model developed by Park and Sung (1997) to heat transfer in separated flows by considering a diffusivity tensor heat transfer model. Several forcing frequencies were employed in simulations at a fixed amplitude (3% of the streamwise time-mean centerline velocity at inlet). They obtained a maximum increase of 40% in the peak value of Stanton number at a specific frequency when compared to the unforced case, suggesting a strong influence of large-scale vortical structures on turbulent heat transfer.

Therefore, the performed literature review reveals that computational analysis of passive scalars in turbulent flows is a promising and growing area. However, most of the numerical predictions are concentrated on boundary conditions that remain invariable during the whole simulation. In the present investigation, the effects of local perturbation of the flow are explored and the mechanisms for drag reduction and heat transfer enhancement are elucidated. DNS over a fully turbulent channel with isothermal walls are carried out and the temperature field is considered a passive scalar.

NUMERICAL DETAILS

The non-dimensional governing equations, i.e., continuity, momentum and passive scalar transport, are:

$$\frac{\partial U_i}{\partial \bar{x}_i} = 0 \tag{1}$$

$$\frac{\partial U_i}{\partial \bar{t}} + \frac{\partial U_i U_j}{\partial \bar{x}_j} = -\frac{\partial P}{\partial \bar{x}_i} + \frac{1}{\mathrm{Re}_h}\frac{\partial^2 U_i}{\partial \bar{x}_j^2} \tag{2}$$

$$\frac{\partial \Theta}{\partial \bar{t}} + \frac{\partial \left(\Theta U_j\right)}{\partial \bar{x}_j} = \frac{1}{\mathrm{Re}_h \mathrm{Pr}}\frac{\partial^2 \Theta}{\partial \bar{x}_j^2} \tag{3}$$

The temperature is non-dimensionalized based on temperatures at the lower hot wall and the upper cold wall. Therefore; based on the present normalization, the values of Θ at the lower and upper walls are +1 and -1, respectively.

The equations of motion have been discretized in an orthogonal coordinate system using a staggered central second-order finite-difference scheme. The discretized system is advanced in time using a fractional-step method, with viscous terms treated implicitly and convective terms explicitly. Details about the numerical procedure are given by Orlandi (2000).

Initial and Boundary Conditions and Input Forcing Parameters

A mean parabolic velocity profile with random fluctuations is applied as initial condition in the entire domain. The no-slip condition is imposed at both walls (except at the local forcing slot). Periodic boundary conditions are assumed along the spanwise and streamwise directions.

Local forcing is modeled as a vertical velocity, V_f, (suction and blowing) with a sinusoidal behavior imposed at both walls in a thin slot of length, L_z, and width, W, equal to $L_x/85$, as shown in to figure 1. Normal perturbing velocities are in phase at both walls. The forcing frequencies are non-dimensionalized by the half height, h, and the centerline laminar velocity, U_C, of the channel (i.e. $\overline{f} = f\,h/U_C$). Integer multiples of the bursting frequency found by Tardu (1998) and Mosyak and Hetsroni (2004) are used in this paper. The bursting frequency (a bursting process is defined as a sharp intensification of production of turbulence in the wall layer) was around 0.011 when non-dimensionalized as $f^+ = f\upsilon/u_\tau^2$. This value corresponds to $\overline{f} = 0.16$ according to our non-dimensionalization. Furthermore, five forcing frequencies are tested: 0.16, 0.32, 0.64, 1.28 and 1.6, which correspond to one, two, four, eight and ten integer multiples of the bursting frequency. The forcing amplitude, $A_o = V_{f\,\max}/U_C$, is fixed at 0.2, where $V_{f\,\max}$ is the maximum normal perturbing velocity.

Both walls are kept at different but constant temperatures. Since the temperature difference is small; buoyancy effects and temperature dependence of the material properties are negligible. Previous considerations and the assumption of incompressible flow support the idea of temperature regarded as a passive scalar.

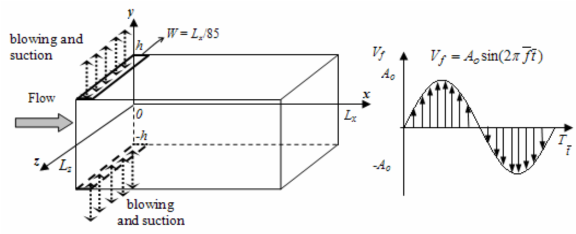

Fig. 1: Schematic of the channel with local forcing.

Phase Averaging Method

When a periodic disturbance is imposed to a domain, the flow can be considered as a superposition of periodic and irregular fluctuations. The disturbed flow is principally dominated by a large-scale structure, according to Hussain and Reynolds (1970). Therefore, the instantaneous quantity, S, can be decomposed into a time mean component, $\overline{S}$, a phase-averaged or coherent component, $\tilde{s}$, and a random or incoherent component, s' :

$$S = \overline{S} + \tilde{s} + s' \tag{4}$$

The time mean component is defined as follows:

$$\overline{S} = \lim_{T\to\infty}\frac{1}{T}\int_0^T S(t)dt \tag{5}$$

A phase-averaging procedure over the instantaneous component, S, gives:

$$\overline{S} + \tilde{s} = \langle S(t)\rangle = \lim_{N\to\infty}\frac{1}{N}\sum_{n=0}^{N} S(t+n\tau) \tag{6}$$

Where N represents the number of periods. Finally, the random or incoherent component, s' , is computed as:

$$s' = S - (\overline{S} + \tilde{s}) \tag{7}$$

NUMERICAL SIMULATIONS

Figure 1 shows the computational domain with the following dimensions: L_z = π, L_y = 2h and L_x = 2π. The mesh configuration is 161x177x257, in the spanwise, normal and streamwise directions, respectively.

The friction coefficient is averaged in time and in the spanwise direction for both walls, whose variation along the streamwise direction is shown in figure 2 for different frequencies in terms of the friction coefficient, $\overline{C_{fo}}$, of the unforced case. Flow perturbation is more pronounced over and at the adjacent downstream zone of the forcing slot, which provokes high velocity gradients; and, consequently, higher skin friction coefficients. Downstream of the source, friction coefficients of forced cases reach a minimum local value (or maximum local drag reduction). An overshoot is appreciated afterward, in the region between $0.08 < x/L_x < 0.4$. As the frequency increases, the maximum local drag reduction also increases and the location of minimum $\bar{c}_f(x)/\bar{C}_{fo}$ moves upstream, closer to the forcing source. This is because the diameter of the spanwise vortex (Park *et al.*, 2003), created by local forcing, is governed by the mass injected during the blowing period and inversely proportional to the frequency. The maximum local skin friction reduction of approximately 30% is achieved at $\bar{f} = 0.64$. The mechanism of drag reduction is explained as follows (Araya *et al.*, 2007): local forcing creates a spanwise vortex downstream of the perturbing source, which generates a reverse flow in the near wall region and reduces the velocity gradient; as a consequence, local drag reduction is accomplished in a determined zone downstream of the source. Finally, the skin friction tends asymptotically toward the friction coefficient of the unforced channel.

As the forcing frequency increases (see distributions at $\bar{f}$ = 1.28 and 1.6 in fig. 2), spanwise vortices shrink and the reverse flow becomes more concentrate and intense at such a point that negative streamwise velocities are obtained with a small separation zone.

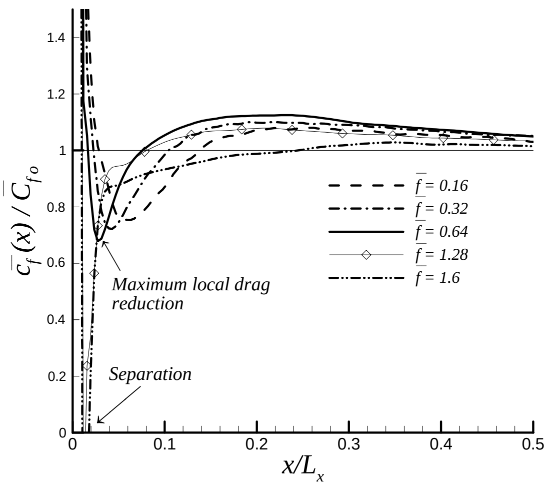

Fig. 2: Relative skin friction coefficient along the streamwise direction at different frequencies.

Figure 3 depicts a comparison of the time-spanwise averaged Stanton numbers between the forced versus unforced cases along the channel. Due to the inherent similarity between the momentum and scalar transport, especially in the vicinity of the wall (Reynolds analogy), the $\bar{s}_t(x)/\bar{S}_{to}$ ratio displays a similar behaviour to the $\bar{c}_f/\bar{C}_{fo}$ coefficient. In the downstream vicinity of the forcing slot ($0 < x/L_x < 0.06$), normal velocities (blowing/suction) provoke high gradients of the thermal field; as a result, increases up to 50% on the Stanton number are found. Profiles experience a sharp decrease downstream; however, Stanton number distribution at $\bar{f} = 0.64$ exhibits much higher values than those of the unperturbed channel in the region $0.06 < x/L_x < 0.5$. Because this particular frequency shows the highest local increase on molecular heat transfer, it is analyzed later in details for turbulent heat fluxes and energy budgets .

All hydrodynamic and thermal components are normalized by the dimensionless friction velocity and dimensionless friction temperature; respectively, which were calculated for the unforced channel, i.e., u_τ = 0.037867 and T_τ = 0.04565. The main reason is to allow a direct comparison between forced and unforced cases.

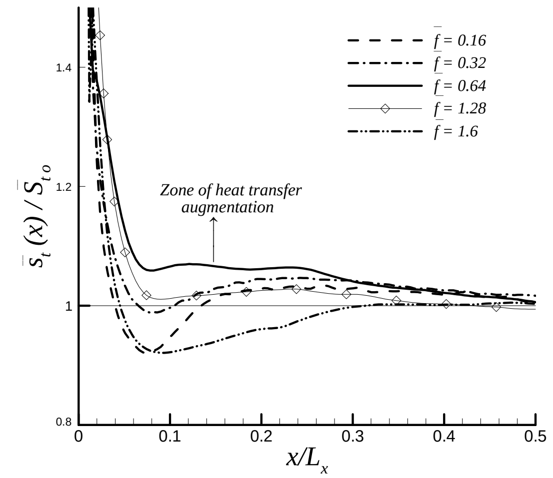

Fig. 3 Relative Stanton number along the streamwise direction at different frequencies.

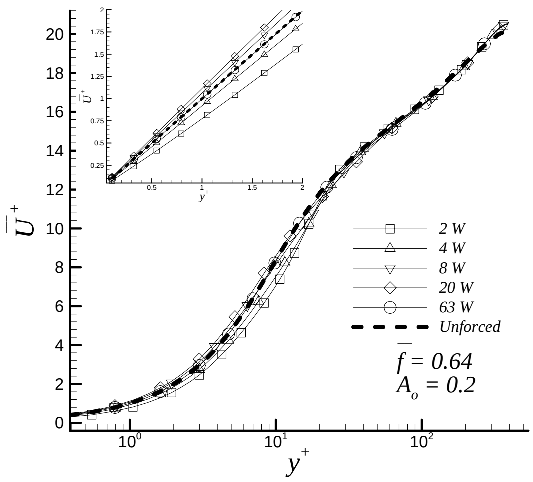

Fig. 4: Time average of streamwise velocity at $\bar{f} = 0.64$.

In fig. 4, the time mean streamwise velocity is plotted at $\bar{f} = 0.64$ and several downstream positions, whose distance to the source are expressed in terms of the slot width, W. A significant distortion is observed in the near wall region and in profiles closer than $20W$ from the source. A zoom of the velocity profiles in the near wall region is plotted in the left upper corner of the image. The lowest velocity gradient is observed at a distance of $2W$, which corresponds to the point of maximum drag reduction.

On the other hand, the effects of local forcing on mean temperature profiles extend up to $y^+ \approx 30$ and in zones near the source, according to fig. 5. The zoom of the near wall region in the left upper corner of fig. 5 reveals higher values of temperature gradients at walls than that of the unforced case. Therefore, higher values of Stanton number are obtained, as well (see distribution at $\overline{f} = 0.64$ in fig. 3). A remarkable deviation from the unforced profile is appreciated in the buffer layer ($10 < y^+ < 30$), which can be atributted to the considerable mixing process taking place in this region. A proof of that is observed in figure 6, where the incoherent component of thermal fluctuations are spanwise averaged and depicted at the instant of maximum injection in the lower wall, when the thermal mixing is more evident. Maximum random fluctuations occur at $y^+ \approx 30$ and at a streamwise distance of $4W$ from the source, and not at the point of maximum drag reduction ($2W$). The reason is that the reverse flow, provoked by the spanwise vortex, attenuates the thermal fluctuations.

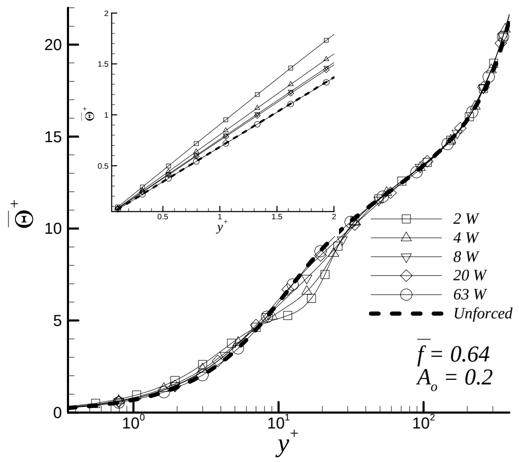

Fig. 5: Time average of temperature at $\overline{f} = 0.64$.

Figures 7a-b show the incoherent component of wall-normal turbulent heat fluxes when averaged only spanwise and spanwise-streamwise, respectively.

In fig. 7a, it is observed that the maximum $\overline{v'^+ \theta'^+}$ develops at around $4W$, a similar behavior is observed in the random thermal fluctuations shown in fig. 6. After performing a spanwise-streamwise averaging process of wall-normal turbulent heat fluxes in fig. 7b, it is possible to infer the net effect of local forcing: a significant increase of $\overline{v'^+ \theta'^+}$ is appreciated from $y^+ \approx 30$ to almost the channel centreline, with a maximum augmentation of 21% in the zone $200 < y^+ < 300$.

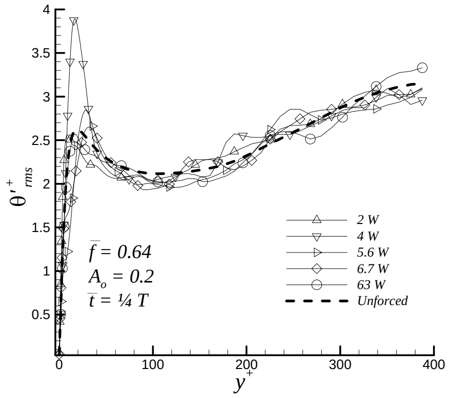

Fig.6: Incoherent component of thermal fluctuations

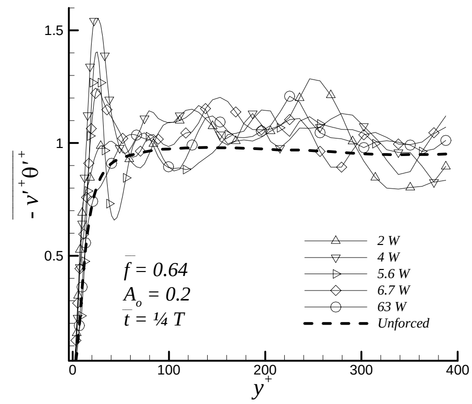

a) Spanwise averaged

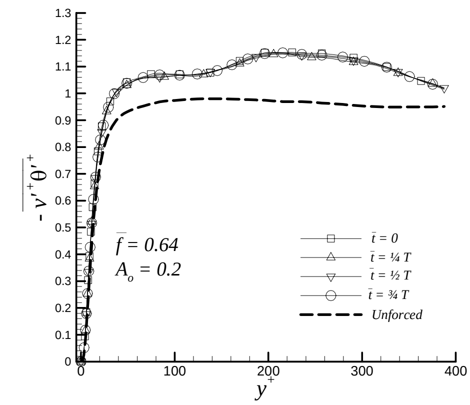

b) Spanwise-streamwise averaged

Fig. 7: Incoherent component of wall-normal turbulent heat fluxes at $\overline{f} = 0.64$.

The coherent component of thermal fluctuations is plotted in fig. 8. High values are seen near the source with a strong damping process along the streamwise direction. At a streamwise distance of $12W$ from the source, coherent thermal fluctuations almost disappear. They are mostly concentrated in the region $0 < y^+ < 30$ and present a strong attenuation toward the channel centreline.

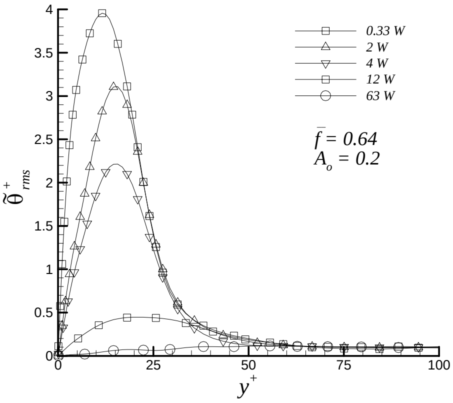

Fig. 8: Coherent component of thermal fluctuations at $\overline{f} = 0.64$.

Budget of the thermal field

A comparison is performed between the thermal budgets of unforced and forced ($\overline{f} = 0.64$) cases. Transport equations of temperature variance and turbulent heat fluxes can be found in Sumitani and Kasagi (1995).

Generally speaking, all terms experience an increase when local forcing is applied in the zone very close to the wall, namely $0 < y^+ < 70$. Beyond this region, the different budget terms of the forced case tend to the values of the unforced case. However, production terms experience a significant increase (and, also, dissipation terms) in the region $200 < y^+ < 300$ (not shown in figures) because of the wall-normal turbulent heat fluxes augmentation in the above mentioned region (see fig. 7b).

Fig. 9 exhibits the budget of the temperature variance, $\overline{\theta'^2}/2$. Molecular diffusion and dissipation undergo a remarkable augmentation, particularly in the near wall region. Increases of approximately 50% are observed at the wall for these terms when compared to the unforced values. The rest of the terms in the budget (namely, production and turbulent diffusion) are almost negligible in the near wall region; therefore, any variation of the molecular diffusion must be accompanied by an opposite variation of the dissipation and vice versa.

Fig. 10 shows the budget of wall-normal turbulent heat fluxes. The pressure-temperature gradient correlation and pressure diffusion terms show increases at the wall for the perturbed channel. However, the highest increases of these terms (~40%) are observed in its peak values at $y^+ \approx 20$ (buffer layer). Another term that undergoes a similar percentage of increase is the production. The increment of dissipation in the region $40 < y^+ < 80$ compensates somehow the production augmentation in this zone. The rest of the terms (turbulent and molecular diffusions) suffer insignificant changes, mostly on their peak values.

Streamwise turbulent heat fluxes depicts small modifications in its budget (see fig. 11). The pressure-temperature gradient correlation term is the most affected with a maximum increase of 35%.

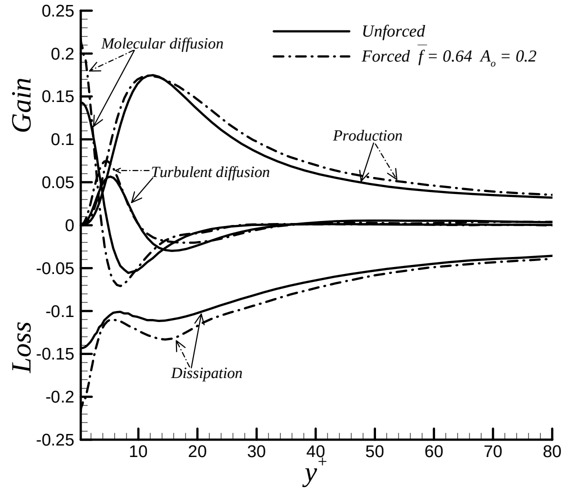

Fig. 9: Budget of temperature variance, $\overline{\theta'^2}/2$.

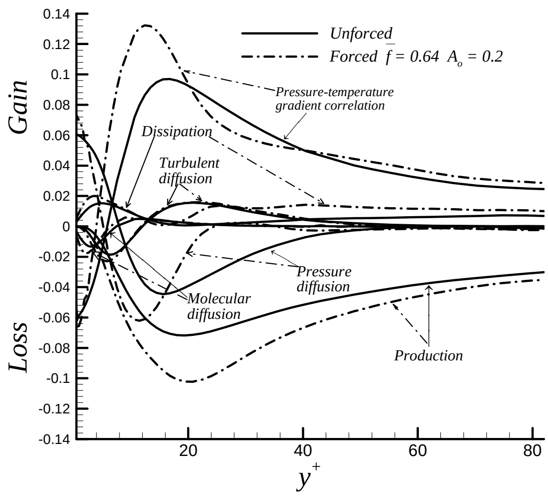

Fig. 10: Budget of wall-normal turbulent heat fluxes.

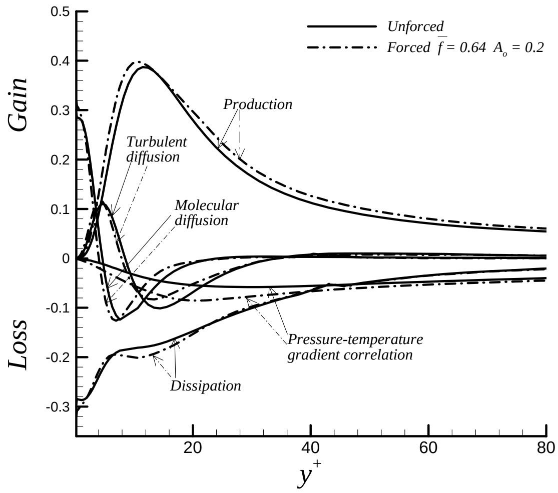

Fig. 11: Budget of streamwise turbulent heat fluxes.

CONCLUSIONS

Based on the wealth of DNS, a detailed analysis of the local forcing influence on the heat transfer in a turbulent channel is introduced. A maximum local drag reduction of 30% together with a Stanton number augmentation up to 50% is achieved at $\overline{f} = 0.64$. In the same way, the wall-normal turbulent heat fluxes are strongly influenced by local forcing with a maximum increase of approximately 21% due to production, pressure-temperature gradient correlation and pressure diffusion terms. For frequencies of 1.28 or higher, spanwise vortices provoke so intense reverse flow that negative streamwise velocities are obtained with a small separation zone.

Coherent thermal fluctuations that arise from the local perturbation of the flow are principally manifested in the vicinity of the slots. They experience a strong damping process not only in the streamwise direction but also in the wall-normal direction due to a rapid lost of momentum. This is the principal difference with the incoherent thermal fluctuations that exhibit peak values near the forcing source, but they tend to the unperturbed channel values far from the slot.

The budget analysis of the temperature variance and turbulent heat fluxes indicates, in general, an increase of all terms when local forcing is applied. Principally, modifications in budget terms by local forcing are induced very close to the wall ($0 < y^+ < 70$). Particularly, molecular diffusion and dissipation of the temperature variance experience a remarkable augmentation at the wall (up to 1.5 times larger than the unforced case values). On the other hand, the budget of wall-normal turbulent heat fluxes shows evidence that maximum increases of pressure-temperature gradient correlation, pressure diffusion and production occur in the buffer layer, which demonstrates the key role of pressure terms in the energy exchange and redistribution among the components.

NOMENCLATURE

A_o: Forcing amplitude
C_p: Specific heat
$\overline{C_f} = u_\tau^2 / U_C^2$: Friction coefficient
ΔT : Temperature difference between walls
$\overline{f}$: Dimensionless frequency
h : Half-height of the channel
L_z, L_y, L_x: spanwise, normal and streamwise dimensions
q_w : Wall heat flux
Re_τ : Reynolds number $\left(= u_\tau h / \upsilon\right)$
$\overline{S_t} = \dfrac{q_w}{\rho C_p U_C \Delta T}$: Stanton number
T : Instantaneous temperature
T : Period ($= 1/\bar{f}$)
T_τ : Friction temperature $\left(= \dfrac{q_w}{\rho C_P u_\tau \Delta T}\right)$
U_C : Laminar Poiseuille centerline velocity
u_τ : Friction velocity $\left(= \sqrt{\tau_w/\rho} \big/ U_C\right)$
V_f : Local perturbing velocity
W : Slot width

Greek symbols
υ : kinematic viscosity
ρ : density
τ_w : shear stress at wall

Superscripts
$\tilde{(\ )}$: Coherent component
( )' : Incoherent component
$(\ )^+$: Wall unit normalization
$\langle\ \rangle$: Phase-averaged
$\overline{(\ )}$: Ensemble average over spanwise direction and time

REFERENCES

Araya, G., Leonardi, S., Castillo, L. and Orlandi, P., 2007, "Direct Numerical Simulations of turbulent channel flow with local forcing at walls", International Journal of Transport Phenomena, accepted for publication.

Bergles, A., Jensen, M., Shome, B., 1995, "Bibliography on enhancement of convective heat and mass transfer", RPI Heat transfer laboratory Report HTL-23.

Gad-el-Hak, M., 2000, "Flow control: passive, active, and reactive flow management", Cambridge; New York Cambridge University Press.

Hussain, A., Reynolds, W., 1970, "The mechanics of an organized wave in turbulent shear flow", J. Fluid Mech., 41, 241-258.

Kim, K., Sung, H., 2003, "Effects of Periodic Blowing from Spanwise Slot on a Turbulent Boundary Layer", AIAA Journal, 41, No. 10.

Mosyak, A., Hetsroni, G., 2004, "Visual study of bursting using infrared technique", Experiments in Fluids, 37, 40–46.

Orlandi, P., 2000, "Fluid Flow Phenomena: A Numerical Toolkit", Dordrecht, Kluwer.

Park, T.S. and Sung, H., 1997, "A New Low-Reynolds-Number Model for Predictions Involving Multiple Surface", Fluid Dynamics Research, vol. 20, pp. 97-113.

Park, Y., Park, S., Sung, H., 2003, "Measurement of local forcing on a turbulent boundary layer using PIV", Experiments in Fluids, 34, 697–707.

Park, Y., Sung, H., 2005, "Influence of local ultrasonic forcing on a turbulent boundary layer", Experiments in Fluids, 39, 966–976.

Rhee, G., Sung, H., 2000, "Enhancement of heat transfer in turbulent separated and reattaching flow by local forcing", Numerical Heat Transfer, Part A, 37, 733 –753.

Sumitani, Y., and Kasagi, N., 1995, "Direct Numerical Simulation of Turbulent Transport With Uniform Wall Injection and Suction", AIAA J., Vol. 33, No. 7, pp. 1220-1228.

Tardu, S., 1998, "Near wall turbulence control by local time periodical blowing", Experimental Thermal and Fluid Science, 16, 41-53.